https://doi.org/10.1016/j.cemconcomp.2022.104700

Effect of dosage of silica fume on the macro-performance and micro/nanostructure of seawater Portland cement pastes prepared with an ultra-low water-to-binder ratio

Yangyang Zhang[a,c,d], *Jun Chang*[e], *Qingxin Zhao*[a,c,d], *Wing Lun Lam*[b], *Peiliang Shen*[b], *Yanjie Sun*[b], *Dahai Zhao*[a,c,d], *Chi Sun Poon* *[,b]

[a]State Key Laboratory of Metastable Materials Science and Technology, Yanshan University, Qinhuangdao, 066004, China

[b]Department of Civil and Environmental Engineering, The Hong Kong Polytechnic University, Hung Hom, Kowloon, Hong Kong, China

[c]Key Laboratory of Green Construction and Intelligent Maintenance for Civil Engineering of Hebei Province, Yanshan University, Qinhuangdao, 066004, China

[d]Hebei Province Low-Carbon and Clean Building Heating Technology Innovation Center, Yanshan University, Qinhuangdao, 066004, China

[e]School of Civil Engineering, Dalian University of Technology, Dalian, 116024, Liaoning, China

*Corresponding author

E-mail: cecspoon@polyu.edu.hk (C.S. Poon)

Abstract

Seawater and sea-sand based ultra-high performance concrete (UHPC) is currently regarded as one of the most innovative and promising construction materials. To provide design guidance for the usage of silica fume (SF) during the production of seawater and sea-sand based UHPC, this work investigated the effect of SF on the later-age macro-performances and micro/nanostructure of seawater ordinary Portland cement (OPC) pastes prepared with a low water-to-binder (W/B) ratio. The results showed that the optimal SF dosage in seawater OPC-SF system was 10 wt.% while that for the deionized (DI) water OPC-SF system was 20 wt.%. This showed that the usage of SF could be reduced for the production of the seawater based UHPC system. It was found that the later-age compressive strength of seawater OPC-SF system was increasingly degraded with increasing SF dosage when compared with the corresponding DI water OPC-SF system. The difference in the distribution of unhydrated clinkers in the matrix as SF addition increased was the main cause. The seawater OPC-10%SF system exhibited the highest compressive strength and the lowest pore content among all the seawater-OPC systems. Additionally, with the usage of this ultra-low W/B ratio, Friedel's salt was only present in the seawater OPC pastes prepared without SF, but absent in the seawater OPC-SF pastes.

Key words: Seawater UHPC; Silica fume; Compressive strength; Micro/nanostructure

1. Introduction

Seawater sea-sand concrete (SSC), as an innovative and sustainable construction material, has attracted increasing research interest worldwide [1-3], especially for coastal cities and remote islands [4]. The shortages of freshwater and river-sand for concrete production have posed challenges to the concrete industry, and thus a novel concept of using seawater and sea-sand instead of freshwater and river-sand together with the use of non-metallic reinforcement (e.g.,

62 fibre reinforced polymer) has been proposed [2, 5, 6]. Some SSC based infrastructures have been
63 successfully applied, for instance, in London's Olympic Stadium, and the Great Belt Bridge
64 located between Denmark and Sweden [3].
65
66 The macro-performance of SSC has been extensively studied in previous research. The usage of
67 seawater would improve the early-age compressive strength of hardened OPC pastes, mortar or
68 concrete [1, 7, 8]. However, the findings regarding the effect of seawater on the later-age
69 compressive strength remain controversial. Kaushik et al. [9] and Younis et al. [10] found that the
70 usage of seawater could slightly lower the later-age compressive strength, while Li et al. [8]
71 reported a similar compressive strength in seawater mixed specimens at 28 days compared with
72 the freshwater mixed specimen. Another study conducted by Wang et al. [5] observed that
73 seawater increased the later-age compressive strength. Generally, most findings have observed a
74 slightly lower long-term compressive strength of SSC compared to ordinary concrete [7, 9-12].
75 Additionally, the usage of seawater reduced the setting time and the initial slump flow, influencing
76 the workability of fresh cement pastes [9, 10]. Regarding the durability of SSC, Nishida et al. [13]
77 stated that the plain concrete structures using seawater as mixing water showed good durability.
78 Younis et al. [10] reported that the usage of seawater slightly increased shrinkage but had little
79 effect on the permeability and Cl^- ion resistance.
80
81 Concerning the microstructure of SSC, the accelerated hydration rates of OPC have been widely
82 observed when concrete was mixed with seawater [5, 7, 8, 14-16]. Wang et al. reported that
83 seawater OPC pastes produced about 1.12 times the cumulative heat generated from deionized

84 water (DI water) OPC pastes during the hydration of 3 days [5]. However, Sikora et al. [15],
85 Montanari et al. [16] and Younis et al. [10] found that the total amount of hydration heat at a
86 medium or later age in seawater OPC pastes was comparable to that in DI water OPC pastes. A
87 similar accelerating effect by seawater can also be seen in the hydration of C_3S [14]. In addition,
88 our previous work suggested that the effect of seawater on accelerating cement hydration was
89 more significant at a lower water-to-binder (W/B) ratio [7]. Previous research also examined the
90 mechanism concerning the accelerating effect of seawater. Edwards et al. demonstrated that the
91 Ca^{2+}, Na^{+}, Mg^{2+}, Cl^{-} and SO_4^{2-} ions in seawater accelerated the hydration of C_3S [17]. Li et al.
92 suggested that the Cl^{-} ion in seawater was the main active ion promoting the precipitation and
93 resulting in the accelerating effect [8]. In addition, using seawater as the mixing water in concrete
94 has also modified the composition of hydration products in OPC pastes. Friedel's salt was
95 observed as the new hydration product in seawater OPC pastes due to the reaction between
96 monosulfate phase and Cl^{-} ion [7, 8]. Wang et al. stated that the formation of Friedel's salt can bind
97 40% of chloride of the seawater [5]. However, Montanari et al. observed that only ~0.47 wt.%
98 Friedel's salt was present in the seawater OPC paste, and most Cl^{-} ions were absorbed in the
99 C-S-H gel [16].
100
101 The accelerating effect of seawater at an early age provides a potential for the production of
102 seawater and sea-sand based ultra-high performance concrete (UHPC). UHPC, as an advanced
103 cement-based material, has a significantly high mechanical strength (typical compressive strength
104 of over 150 MPa and tensile strength of over 20 MPa) and excellent durability [18-20]. Generally,
105 UHPC comprises cement, fine supplementary cementitious materials, quartz sand, fibers, water at

a very low W/B ratio, and superplasticizers [21, 22]. Due to the use of a high dosage of superplasticizer to assure workability at a low W/B, the early hydration and strength development can be retarded. The usage of seawater can improve the retarded hydration and the early-age mechanical strength of UHPC. Teng et al. produced seawater and sea-sand UHPC at a W/B ratio of 0.18, which was prepared with a 52.5N OPC, silica fume (SF), quartz powder and superplasticizer. The UHPC had a compressive strength of over 180 MPa [4]. Shi et al. examined the effect of seawater on the early-age (3 days) hydration of cement with the incorporation of slag and SF at a W/B of 0.2, and showed that seawater increased the early-age compressive strength of the specimens, modified the interaction of slag and SF, and decreased the reactivity of SF [23]. However, few studies have investigated the influence of seawater on the later-age (≥28 days) macro-performance and microstructure of OPC with SF at low W/B. Moreover, the research regarding seawater OPC-SF pastes prepared with a very low W/B ratio is limited. Furthermore, the evolution of macro-performances and microstructure of seawater OPC pastes with different SF addition need to be investigated, which is beneficial to provide some recommendations for the appropriate SF content in seawater and sea-sand based UHPC.

This work presents an experimental study on the influence of SF on the later-age compressive strength, impedance modulus and micro/nanostructure of seawater OPC pastes prepared with an ultra-low W/B ratio. The evolutions of macro-performances, hydration process and hydration products of a cement paste prepared with a W/B ratio of 0.15 and different SF replacements ranging from 0 wt.% to 30 wt.% of the total binders were investigated. The aim was to identify the effect of seawater on the most optimal dosage of SF in the OPC-SF system.

2. Materials and experimental procedure

2.1 Materials

In this study, an ASTM Type I OPC and a SF produced by Elkem (China) were used. Table 1 shows the chemical composition of SF and OPC, tested by X-ray fluorescence spectroscopy (Supermin200, Rangaku Corporation, Japan). Fig. 1 shows the XRD results of SF and OPC. The SF was amorphous, and the composition of OPC was 66.4 wt.% of C_3S, 11.9 wt.% of C_2S, 6.0 wt.% of C_3A, 7.2 wt.% of C_4AF, 5.8 wt.% of $CaCO_3$ and 2.7 wt.% of gypsum. Table 2 shows the ICSD codes used for the Rietveld analysis. The polycarboxylate-based superplasticizer (with a solid content of 20%) produced by BASF was used. The artificial seawater was prepared according to ASTM D1141-98 (2013), as shown in Table 3.

Table 1 Chemical composition of SF and OPC (wt%)

Phase	CaO	SiO_2	Al_2O_3	Fe_2O_3	SO_3	MgO	K_2O	TiO_2	P_2O_5	ZnO	MnO	CuO	Cl	SrO	ZrO_2
SF	0.73	95.7	0.45	0.07	0.27	0.71	1.74	-	0.09	-	0.03	-	0.22	-	-
OPC	66.10	20.00	5.13	3.24	2.99	1.09	0.60	0.27	0.24	0.10	0.08	0.05	0.04	0.04	0.01

-: not detected.

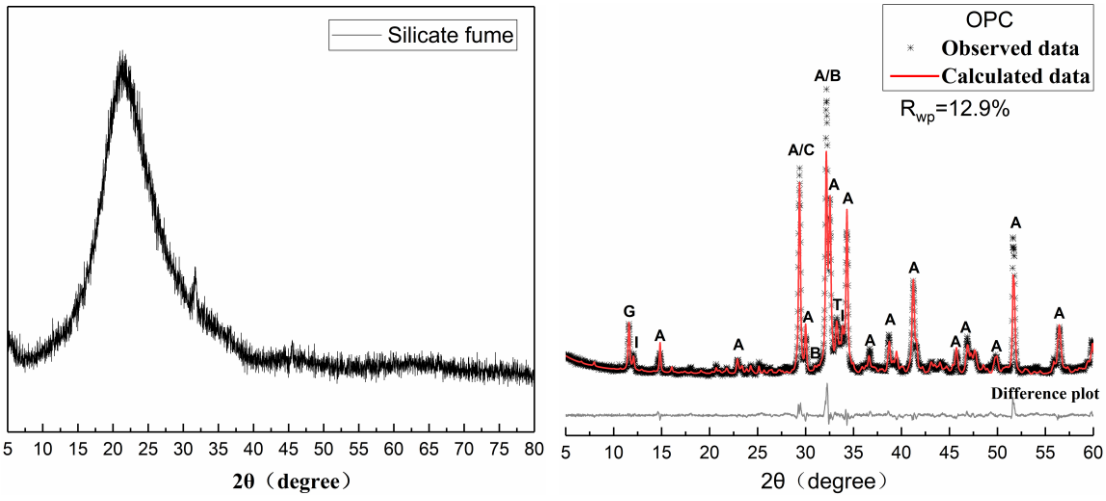

Fig. 1 XRD curve of SF and Rietveld quantitative analysis for OPC. Legend: A: C_3S; B: C_2S; T: C_3A; I: C_4AF; C: $CaCO_3$; G: gypsum.

Table 2 Phase compositions and ICSD codes used for quantitative analysis.

Phase	ICSD Codes
C_3S	4331
C_2S	81096
C_3A	1841
C_4AF	9197
$C\check{S}H_2$	36186
$CaCO_3$	18165
CH	34241
AFt	155395
Friedel's salt	62363
Al_2O_3	10425

Table 3 Compositions of the artificial seawater (g/L)

Type	NaCl	$MgCl_2$	Na_2SO_4	$CaCl_2$	KCl	$NaHCO_3$	KBr
Concentration	24.53	5.20	4.09	1.16	0.695	0.201	0.101

2.2 Specimen preparation

In order to investigate the effect of SF on the seawater OPC pastes prepared at a low W/B ratio, different contents of SF, a W/B ratio of 0.15 and a superplasticizer dosage of 3 wt% of the total binders were used to produce the specimens. The pastes were mixed with DI and seawater, respectively. Table 4 shows the detailed mix proportions.

Based on the modified Andreasen & Andersen model [24], the grading curves of the different cement paste mixes and the target curve were obtained to theoretically investigate the evolution of the pore structures, shown in Fig. 2. The target curve was developed by using the Least Squares Method to adjust the contents of OPC and SF and optimize the packing [24]. The most theoretically favorable particle distribution among the mixes was observed when 20 wt% SF was

incorporated.

Table 4 Mixture design of different pastes

Sample	D0	D10	D20	D30	S0	S10	S20	S30
OPC (wt%)	100	90	80	70	100	90	80	70
SF (wt%)	0	10	20	30	0	10	20	30
Mixing water	DI water	DI water	DI water	DI water	seawater	seawater	seawater	seawater

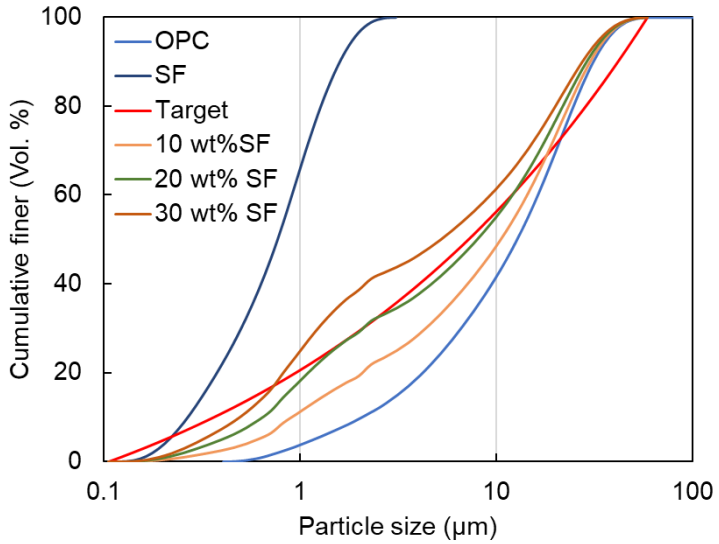

Fig. 2 Particle size distributions of SF, OPC, target grading curve, and the grading curves with different SF contents.

The cementitious materials (i.e., OPC and SF) were dry mixed for 1 min at a low speed before adding DI water or seawater and the superplasticizer. The pastes were then mixed for 1 min at low speed and 5 min at high speed. The well-mixed pastes were cast into 40 mm × 40 mm × 40 mm steel cube molds, and vibrated on a mechanical vibration table for 1 min. Then, the samples were covered with plastic films and cured at 23 ± 2 °C for 24 h. After demolding, the samples were cured at 23 ± 2 °C and >95% relative humidity until testing. Fig. 3 shows the picture of paste

specimens. The compressive strength test was then performed at the testing ages with a loading rate of 0.96 kN/s. The broken samples after the compressive strength test were collected and grounded into powder or small particles, and then immersed in isopropanol and vacuum dried for microstructure analysis [25].

Fig. 3 Picture of paste specimens

2.3 Microstructure methods

Electrochemical impedance spectroscopy (EIS) was conducted using a Multi-AutolabM 204 instrument where its frequency ranged from 10 mHz to 1 MHz and its AC signal magnitude was 10 mV. The samples were dried with a towel, covered by two thin wet sponges, and immediately measured using a two-electrode system. The resulting impedance spectra were analyzed by Nova 1.11 software.

X-ray diffraction (XRD) curves were acquired using a Bruker D8 Advance X-Ray Powder Diffractometer (Germany) equipped with CuKa12 radiation (λ_1 = 0.15406 nm, λ_2 = 0.15444 nm) under the conditions of 40 kV tube voltage and 40 mA tube current. The measurement was set with the step size at 0.020°, the rate of 0.5 s per step and the 2θ ranging from 5.0° to 80.0°. The

overall measurement time was about 30 min to ensure the favorable signal-to-noise ratio. TOPAS 5.0 software was used for quantifying each mineral content of OPC and hydration products. To prepare the samples for the experiment, the hydrated powder was well mixed with 10 wt% α-Al_2O_3 (Aladdin, 99.99% purity) as an internal standard to calculate the content of amorphous (Acn) phases and crystalline phases. The overall refined parameters included background coefficients, zero-shift error, phase scale factors, Chebyshev polynomial correction, Lorentz polarization factor, crystal structures and cell parameters. The ICSD codes used for quantitative analysis were shown in Table 2.

Thermogravimetric (TG) curves were recorded using a Mettler Toledo TGA/DSC1 instrument. The heating procedure was set from 30°C to 1000°C at a constant heating rate of 10°C/min. 10 ± 0.5 mg test powder was put into a corundum crucible and heated under N_2 atmosphere.

Nitrogen adsorption and desorption curves were acquired using an ASAP 2020 Micromeritics Accelerated Surface Area and Porosimetry instrument. The test powder was firstly degassed and preheated at 60 °C and at a pressure of 0.1 mmHg for 24 h. The bath temperature for analysis was -196 °C. The pore volume distribution was obtained based on Barrett-Joyner-Halenda (BJH) analysis.

Mercury intrusion porosimeter (MIP) analysis was conducted using a Micromeritics AutoPore IV 9500 Series instrument where the maximum mercury intrusion pressure was 207 MPa. The specimens were broken into small particles with a size of ~5 mm and soaked in isopropanol as an

exchange solvent. Finally, the specimens were dried in a vacuum desiccator for 7d before the MIP analysis.

^{29}Si magic angle spinning nuclear magnetic resonance (^{29}Si MAS-NMR) curves were recorded using a GEOL 500 MHz spectrometer with a 7-mm CP/MAS probe. The rotation rate and resonance frequency for the measurement were set at 4500 Hz and 79.5 MHz, respectively. The relaxation delay was 30 s and over 2000 scan was completed for each ^{29}Si MAS-NMR spectrum.

Backscattered electron (BSE) images were performed by a Tescan VEGA3 instrument with an accelerating voltage of 20 kV. Firstly, the dried samples were mounted in the low-viscosity epoxy resin (EPO-TEK 301) under a vacuum pressure of 10 mbar, ensuring that the air was removed and the epoxy resin was infiltrated well. After the epoxy was solidified (~24h), the mounted specimens were polished by a grinding & polishing equipment (Buehler AutoMet 300)/ the details of the procedures were modified according to the previous work [26], and isopropanol was used at the first step. The polished samples were coated with carbon prior to BSE measurements.

Nanoindentation was performed using a Hysitron Triboindenter 950 system (TI 950 TriboIndenter, Bruker) equipped with a Berkovich diamond indenter probe. Firstly, the surface roughness of the chosen area was determined to ensure it was lower than 70 nm for nanoindentation measurement [27]. For the analysis, a 15 × 15 grid with a 10 μm interval was chosen, and therefore 225 indentations in total were determined. The peak load was set at 2000 μN, with a period of 10 s loading time, 5s holding time, and 10s unloading time. The elastic modulus (Er) of each

indentation was determined based on the previous guidelines [28].

3. Results

3.1 Compressive strength

Fig. 4 shows the compressive strength of seawater and DI water OPC pastes with different SF contents. Compared to DI water OPC pastes, the seawater OPC pastes with each SF addition showed a higher compressive strength at 1 day due to the presence of active ions in the seawater. The higher early-age compressive strength of seawater OPC pastes without SF was also confirmed by previous works [1, 5, 7, 8]. In addition, the compressive strength of seawater was significantly improved at an early age when the used SF content was 30 wt%. However, the compressive strength of seawater OPC pastes was lower at 7 and 28 days compared to DI water OPC pastes. Furthermore, the decreasing rate in compressive strength was much higher as the increase in SF content, i.e., 2.9% (0 wt% SF), 5.3% (10 wt% SF), 20.8% (20 wt% SF), 27.3% (30 wt% SF), and thus the addition of SF would further decrease the later-age compressive strength of the seawater OPC pastes.

In addition, the compressive strength evolution of DI water OPC pastes and seawater OPC pastes with different SF contents was determined. In Fig. 4, the compressive strength of DI water and seawater group increased firstly and then decreased with increasing SF contents. The highest compressive strength (~105 MPa) of DI water OPC pastes was observed when incorporating 20 wt% SF, while the seawater OPC pastes with 10 wt% SF showed the highest compressive strength (~98 MPa). Furthermore, with respect to the OPC-based construction materials used an ultra-low

W/B, the usage of seawater can reduce production costs as the seawater OPC-SF system with a low SF addition would have the highest macro-strength, saving SF dosage.

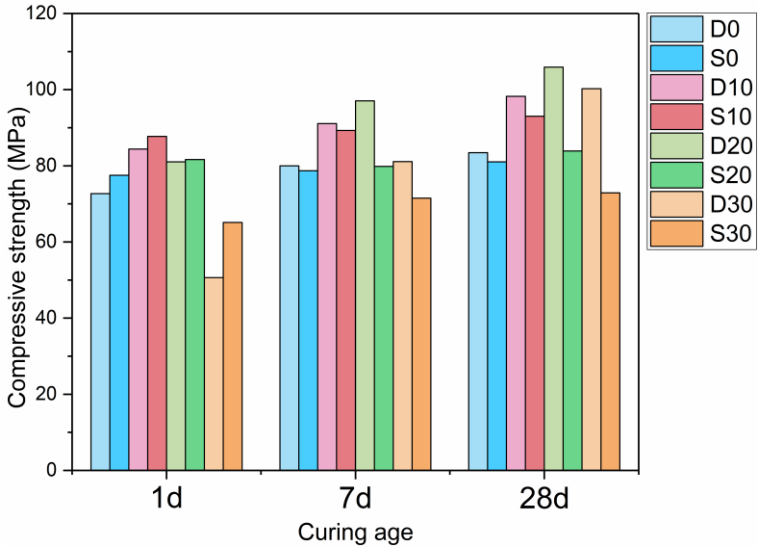

Fig. 4 Compressive strength of different specimens at 1, 7 and 28 days

3.2 EIS measurements

Fig. 5 shows the results of the electrochemical impedance test of seawater and DI water OPC pastes with different SF contents. The impedance modulus changes with the change of ion transport properties in concrete. The ion transport rate would be slower as the impedance modulus increases, and thus ions in the external environment would be harder to enter the interior of the specimen, suggesting that the specimen would exhibit a favorable durability. In both DI water pastes and seawater pastes, the addition of SF decreased the impedance modulus at 1day, and the impedance modulus was further decreased with increasing SF content. However, after curing for 7 or 28 days, the impedance modulus of the specimens with SF was higher compared to that without SF. In addition, the impedance modulus significantly increased with SF content or with prolonged curing age, corresponding to the improvement in external ions corrosion resistance.

The comparison of impedance modulus of seawater OPC pastes and DI water OPC pastes is shown in Fig. 6. Specimens without SF in DI water and seawater group showed a similar impedance modulus. The scenario was different when incorporating SF. The impedance modulus of S10 and S20 were higher than that of D10 and D20, respectively. However, S30 had a lower impedance modulus compared to D30. Therefore, seawater can increase the impedance modulus when 10 wt.% and 20 wt.% SF were used, indicating that the durability of those two seawater OPC-SF systems was improved compared with the corresponding DI water systems.

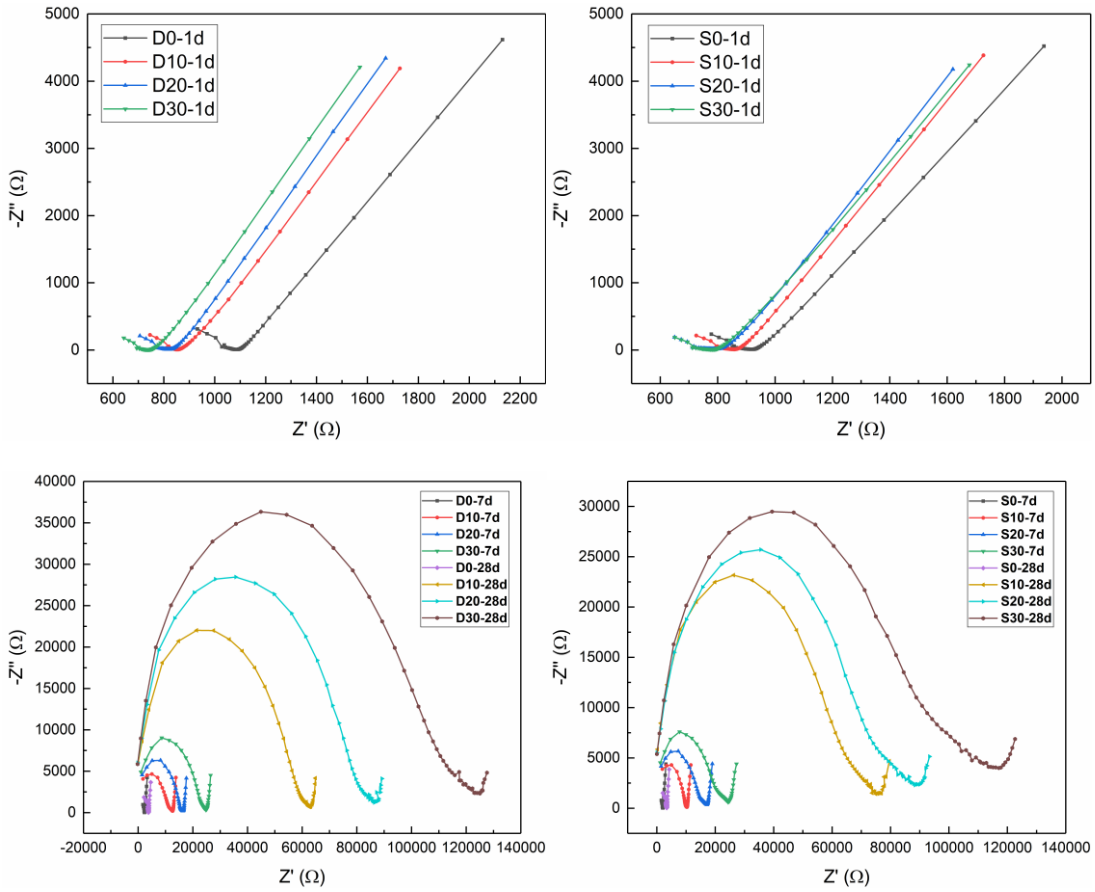

Fig. 5 EIS results of different samples at 1, 7 and 28 days

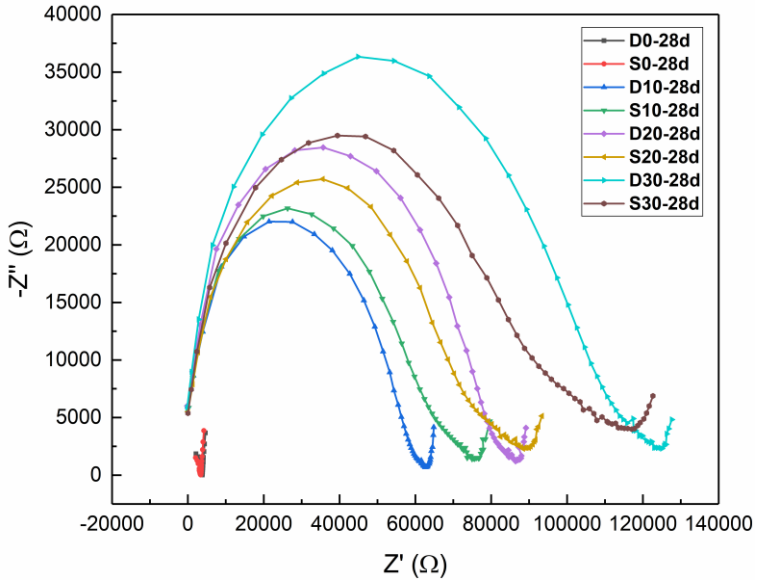

Fig. 6 Comparison of seawater and DI water OPC pastes at 28 days

3.3 Compositions and contents of hydration products

The compositions of hydration products were analysed by XRD using EVA software. Fig. 7 shows the XRD patterns of seawater OPC pastes and DI water OPC pastes at 1, 7 and 28 days. The unhydrated clinkers (C_3S, C_2S, C_3A, C_4AF and $CaCO_3$) could be clearly observed as their peaks were easily identified at the ultra-low W/B. The XRD peaks of main crystalline hydration products (i.e., AFt and CH) were identified in both seawater and DI water OPC pastes, which was also confirmed by the TGA-DTG curves in Fig. 8. Due to the presence of Cl^- in seawater, Friedel's salt ($Ca_4Al_2(OH)_{12}Cl_2 \cdot 4H_2O$), as a Cl-containing crystalline product, was obviously detected in S0 sample at 7 or 28 days, which was consistent with previous works [5, 29, 30]. Gypsum peaks were not detected at both the early or later age and this might indicate that gypsum was easily dissolved and reacted with C_3A and Cl^- to form AFt and Friedel's salt.

The incorporation of SF influenced the compositions of hydrated seawater OPC pastes. As shown in Fig. 7, Friedel's salt was hardly detected at 7 or 28 days when SF was used, and can only be found in the S0 sample. Previous works suggested that Cl^- ion can be physically absorbed in the structure of C-S-H gel [16, 31-34], and Cl^- tended to attach to C-S-H gel due to high absorbability instead of participating in the formation of Friedel's salt [16]. This might be due to with the presence of SF, more C-S-H gel with a low Ca/Si ratio was formed. This type of C-S-H gel and SiO_2 gel exhibited a high specific surface area for physical absorption of Cl^- ion, and thus less free Cl^- ion participated in the formation of Friedel's salt.

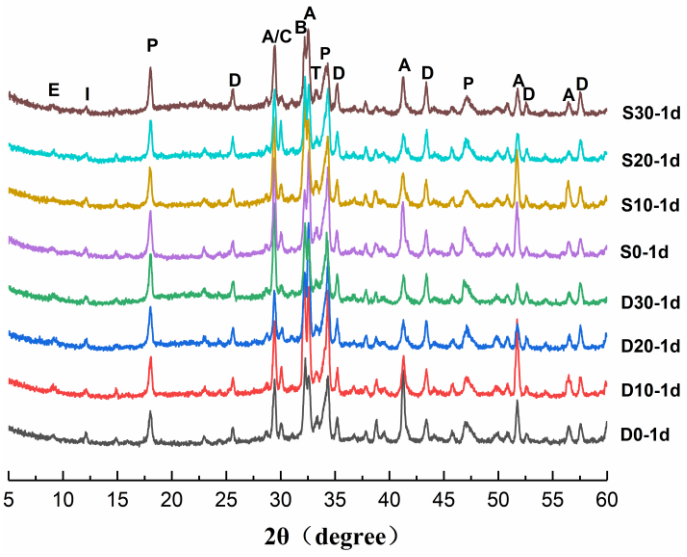

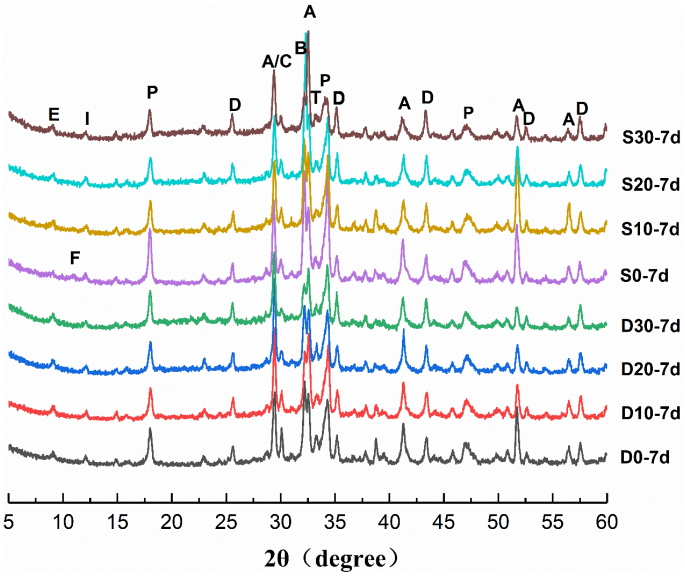

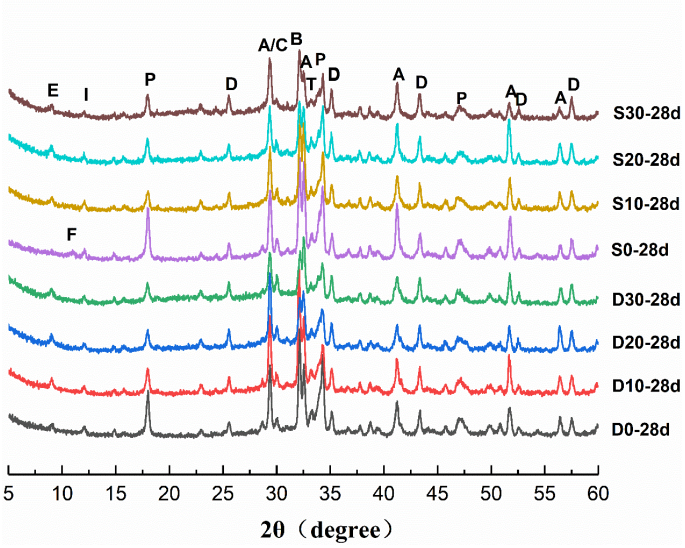

Fig. 7 XRD patterns of samples at 1, 7 and 28 days.

Legend: E: ettringite (AFt); F: Friedel's salt; P: CH; A: C_3S; B: C_2S; T: C_3A; I: C_4AF; C: Calcite; D: Al_2O_3.

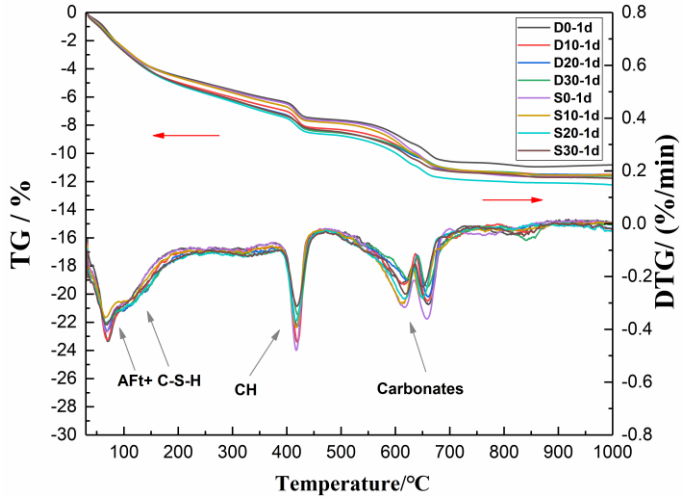

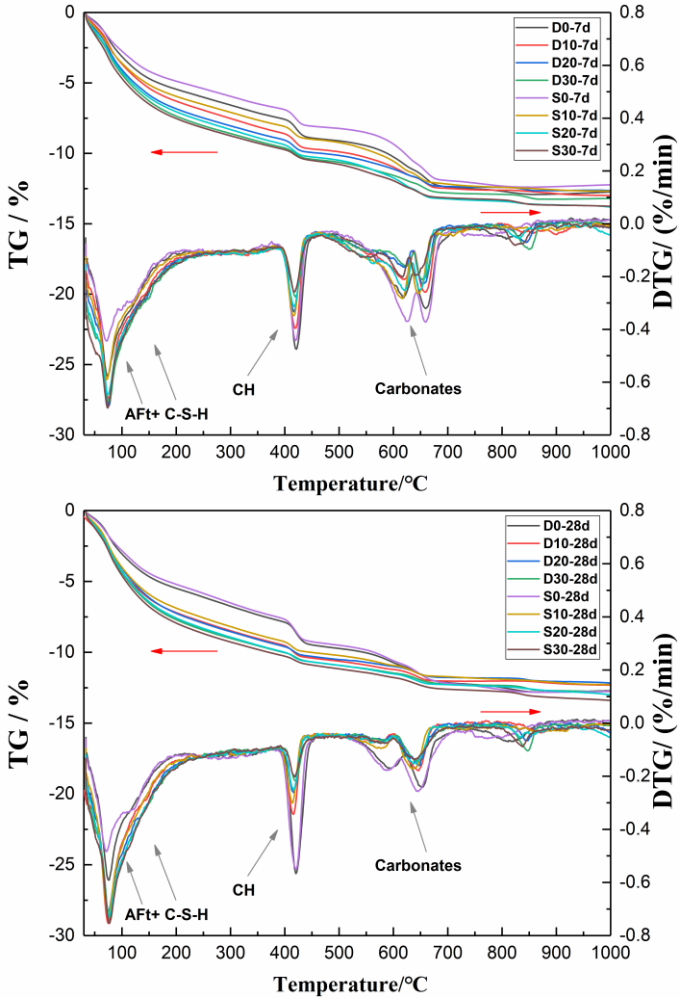

Fig. 8 TG-DTG curves of different samples at 1, 7 and 28 days

The contents of unhydrated clinkers and hydration products were determined by the Rietveld method. Table 5 shows the quantitative XRD results of the samples at 1 and 28 days. All R_{wp} (weighted-profile R value) values were lower than 15%, corresponding to the good accuracy of quantitative results. Additionally, the Rietveld plots of D30 and S30 samples at 28 days, as two typical examples, were shown in Fig. 9. Firstly, seawater accelerated the early-age hydration rate of OPC-SF system. The hydration degree of C_3S (the principal early-hydration clinker phase) was increased at 1 day in all the seawater OPC-SF systems. The higher CH content (8.6 wt%) at 1 day in S0 specimen (Table 5) and the higher mass loss of CH (Fig. 8) in S0 supported the observation. In addition, the seawater OPC pastes prepared with SF incorporation exhibited a lower CH content

at 1 day compared to the DI water OPC pastes with SF shown in Table 5, indicating that seawater also accelerated the pozzolanic reaction between CH and SF at an early age. However, the accelerating effect of seawater was not obvious in the OPC pastes prepared without SF or with only 10 wt% SF at a later age. The C_3S content and the mass loss of CH at 28 days were similar in S0 and D0, and S10 and D10 samples (Table 5). However, S30 showed a lower C_3S content and higher Acn content compared to D30, indicating that the acceleration effect of seawater was still observed when 30 wt% SF was used. The acceleration effect of seawater mainly occurred at an early age, while the cumulative heat release of the seawater mixed paste was comparable to that of the freshwater mixed paste after 7 days [5, 16, 35, 36]. Also, the low W/B used in the UHPC might have also reduced the acceleration effect at a later age. But this study showed that seawater accelerated the pozzolanic reaction, and this acceleration effect might be more obvious with a higher SF dosage. Thus, the acceleration effect of seawater was still found in S30 sample at a later age.

The change of Friedel's salt content was further quantitatively determined in the seawater OPC-SF system (Table 5). Friedel's salt was absent in all OPC-SF systems at 1 day, while it was present in the S0 specimen at 28 days. However, the AFt content was significantly increased in the seawater OPC pastes prepared with SF. The above observation was consistent with the fact that C-S-H gel with a low Ca/Si ratio and SiO_2 gel would absorb Cl^- ion, and the aluminate ions ($Al(OH)_4^-$) would react with sulfate ions (SO_4^{2-}), forming more AFt.

Table 5 Quantitative XRD results at 1 and 28 days. (wt%)

Sample	C_3S	C_2S	C_3A	C_4AF	Calcite	CH	AFt	F salt[a]	Acn	R_{wp}	Clinkers[b]	Hydrates[c]
D0-1d	39.2	12.5	3.8	4.9	4.9	7.3	2.9	-	24.5	11.0	65.3	34.7
D10-1d	36.3	11.2	2.9	5.4	4.4	6.6	2.5	-	30.7	10.3	60.2	39.8
D20-1d	22.4	12.7	2.2	5.5	3.9	5.4	2.4	-	45.5	10.6	46.7	53.3
D30-1d	21.0	10.5	2.5	3.4	3.7	4.6	2.1	-	52.2	10.1	41.1	58.9
S0-1d	33.1	11.1	3.7	4.9	5.4	8.6	2.4	-	30.8	11.1	58.2	41.8
S10-1d	32.7	11.3	3.0	4.2	4.1	5.4	1.0	-	38.3	10.0	55.3	44.7
S20-1d	20.3	11.4	1.3	5.1	4.2	5.2	1.9	-	50.6	10.6	42.3	57.7
S30-1d	16.0	10.6	1.8	4.7	3.5	3.5	2.1	-	57.8	10.1	36.6	63.4
D0-28d	27.9	12.1	2.9	6.5	4.7	7.8	2.1	-	36.0	9.9	54.1	45.9
D10-28d	26.8	11.1	2.5	4.9	4.5	4.3	4.0	-	41.9	10.2	49.8	50.2
D20-28d	20.4	10.3	1.8	4.0	4.2	3.4	3.3	-	52.6	10.5	40.7	59.3
D30-28d	20.7	8.9	1.4	3.8	4.2	2.0	3.4	-	55.6	11.3	39.0	61.0
S0-28d	28.0	11.2	2.3	6.5	4.8	8.4	1.0	2.0	35.8	10.4	52.8	47.2
S10-28d	26.3	11.2	1.4	5.1	4.2	3.9	3.2	-	44.7	10.5	48.2	51.8
S20-28d	17.7	10.2	2.4	3.9	3.6	3.3	3.6	-	55.3	10.9	37.8	62.2
S30-28d	15.1	8.3	2.0	4.1	3.5	1.7	4.3	-	61.0	11.2	33.0	67.0

-: not present.

[a]: Friedel's salt

[b]: content of total unhydrated clinkers

[c]: content of total hydration products

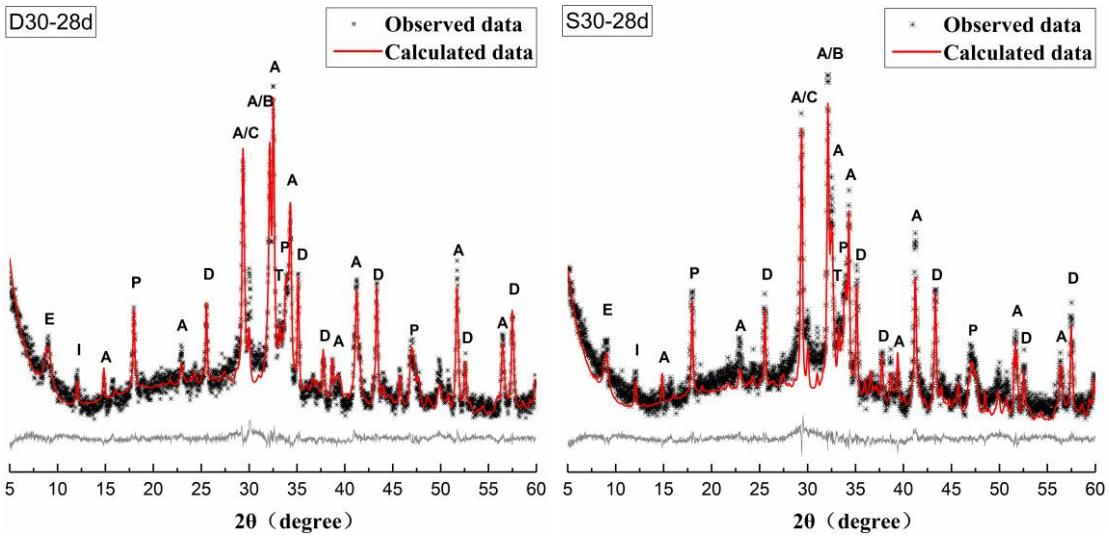

Fig. 9 Rietveld quantitative analysis for D30-28d and S30-28d. Legend: E: ettringite (AFt); P: CH; A: C_3S; B: C_2S; T: C_3A; I: C_4AF; C: Calcite; D: Al_2O_3.

3.4 ^{29}Si MAS-NMR measurements

The nanostructures of C-S-H gel and SiO_2 gel were analyzed using the ^{29}Si MAS-NMR spectra. The usage of seawater and SF changed the structure of the C-S-H gel. Fig. 10 shows the ^{29}Si MAS-NMR spectra of seawater and DI water OPC pastes prepared without SF and with 30 wt.% SF at 28 days, including the raw experimental, deconvoluted, and different Q^n (where n ranges from 0 to 4) structural unit curves. Q^n represents different Si-O tetrahedron structures, and n denotes the number of oxygen bridges. Generally, the ^{29}Si MAS-NMR spectra exhibit five signals of Q^n Si-O tetrahedron structures, including (a) Q^0 located at -68 to -75 ppm that represents the uncondensed silicate group (monomer), (b) Q^1 located at -76 to -82 ppm that represents the chain-end silicate group of C-S-H gel, (c) Q^2 located at -82 to -88 ppm that represents the chain-middle silicate group of C-S-H gel, (d) Q^3 located at -88 to -98 ppm that represents the layers and chain branching sites of the silicate group of amorphous SiO_2 gel, and (e) Q^4 located at -98 to -120 ppm that represents the three-dimensional networks layers of the silicate group of amorphous SiO_2 gel [37-39].

The deconvoluted curves were derived from the Gauss and Lorentz type component convolutions using Peakfit 4.12 software, shown in Fig. 10. Table 6 summarizes Q^n distributions, and calculated polymerization degree, mean molecular chain length and fraction of vacant tetrahedral sites of the C-S-H gel. In Fig. 10, the D0 and S0 samples exhibited three ^{29}Si MAS-NMR signals (viz. Q^0, Q^1 and Q^2), and Q^3 or Q^4 signals were not present, further confirming that no supplementary cementitious materials were present in this OPC paste. Also, Q^0, the signal for siliceous clinkers, accounted for over 80%, because of the low hydration degree at this low W/B. S0 sample had a

similar percentage of Q^0 compared to D0 sample, suggesting the similar hydration degrees of the two samples. S30 exhibited an evidently lower percentage of Q^0 compared to D30 sample, demonstrating a higher hydration degree than D30 sample. The sum of Q^1 and Q^2, as two characteristic signals of C-S-H gel, further confirmed the change of hydration degree in the seawater and DI water OPC pastes, which was also consistent with the Rietveld quantitative analysis results (Table 5).

The structure of C-S-H gel changed with the usage of SF and seawater as shown in Table 6. In both seawater OPC pastes and DI water OPC pastes, the polymerization degree and mean molecular chain length of C-S-H gel increased with the presence of SF, and an opposite trend was observed regarding the fraction of vacant tetrahedral sites of C-S-H gel. The observation was attributed to the formation of the C-S-H gel with a low Ca/Si ratio by the reaction of SF and CH, and this C-S-H gel had a higher polymerization degree and a longer molecular chain length. In addition, the polymerization degree and mean molecular chain length of the C-S-H gel in the seawater OPC and OPC-30%SF systems were lower than those in DI water OPC and OPC-30%SF systems, indicating that the usage of seawater changed the Ca/Si ratio of C-S-H. The difference in the C-S-H structure was due to the presence of sodium ions in seawater, which influenced the C-S-H structure. Sodium ions substituted the calcium ions in C-S-H structure and were incorporated on the C-S-H surface or in the C-S-H interlayer. Thus, the C-S-H structure was reorganized, resulting in a decrease of mean molecular chain length [7, 40].

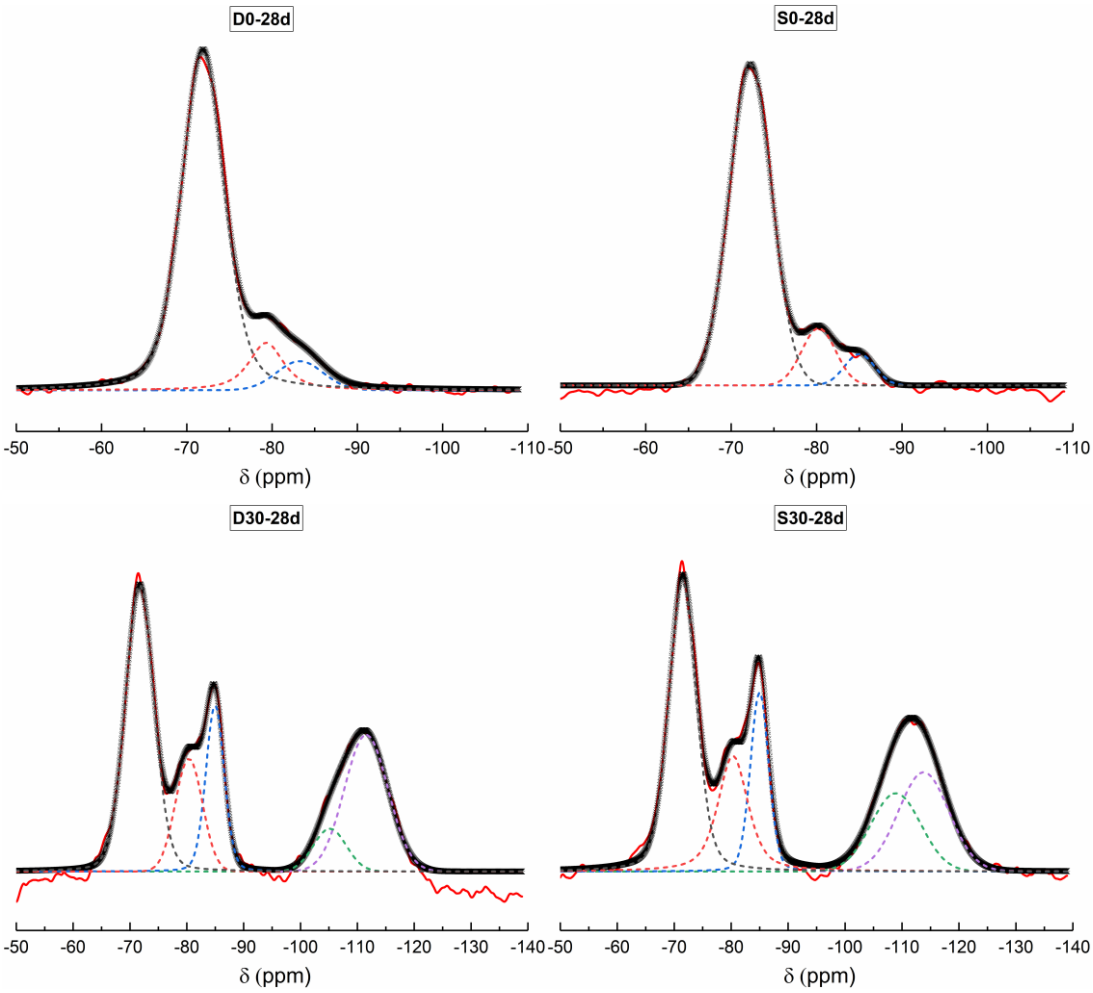

Fig. 10 ^{29}Si MAS-NMR spectra of different hydrated pastes at 28 days.

Table 6 Percentages of Q^0, Q^1, Q^2, Q^3 and Q^4 resonances and characterization parameters of C-S-H structure

Sample	Q^0(%)	Q^1(%)	Q^2(%)	Q^3(%)	Q^4(%)	PD[a]	MCL[b]	v[c]
D0-28d	82.42	10.90	6.68	-	-	0.61	3.22	0.24
S0-28d	81.60	12.71	5.69	-	-	0.45	2.90	0.26
D30-28d	39.08	13.62	14.58	6.58	26.44	1.07	4.14	0.19
S30-28d	34.73	16.91	13.62	15.02	19.72	0.81	3.62	0.22

-: not present.

[a] Polymerization degree of C-S-H, PD = Q^2/Q^1. [37]

[b] Mean molecular chain length of C-S-H, MCL=$2(Q^1+Q^2)/Q^1$. [37, 38]

[c] Fraction of vacant tetrahedral sites, v = 1/(MCL+1). [41]

3.5 Pore structure

Nitrogen adsorption and desorption measurements were used for the analysis of the pore structure of the cement pastes ranging from 2 nm to 20 nm. MIP measurements were used for analyzing the

pore structure ranging from 20 nm to 1000 nm. Fig. 11 shows the BJH adsorption pore volume and dV/dD pore volume of D0, S0, D30 and S30 samples at 28 days. S0 sample exhibited a smaller nanopore size between 2 nm and 20 nm compared to D0 sample since seawater accelerated the hydration reaction. However, S30 sample shows a similar but slightly smaller pore size distribution compared to D30 sample. Thus, the effect of seawater on the nanopore size was reduced when SF was used.

Fig. 12 shows the MIP results of D0, S0, D30 and S30 samples at 28 days. It is obvious that the cumulative pore area with a pore diameter of 35 nm or more in S0 sample was invariably higher than that of D0 sample, but the cumulative pore area with a pore diameter between 20 nm - 35 nm of D0 sample was substantially increased, and was higher than that of the S0 sample. Additionally, the major pore size fraction of D0 was located at ~40 nm, which was smaller compared with S0 sample (its peak was located at ~45 nm). Also, the average pore diameter and median pore diameter of S0 sample were 53.7 nm and 49.1 nm, respectively, which were higher than those of the D0 sample with an average pore diameter of 43 nm and a median pore diameter of 41.8 nm. With the usage of 30 wt% SF, the seawater OPC pastes and DI water OPC pastes exhibited a very fine pore structure, e.g., the total cumulative pore areas of D30 and S30 samples were extremely low (less than 0.5 m^3/g).

Combining the results of nitrogen adsorption and desorption measurements and MIP provided the information of the pore structure in the size range of 2 nm – 1000 nm. The usage of seawater decreased the amount of pore between 2 nm and 20 nm, but increased the content of pore ranging

from 20 nm to 1000 nm when SF was not used. It was due to the accelerated hydration of seawater, leading to pore coarsening (decrease in finer pores and increase in larger pores). This resulted in an inferior pore size distribution. With SF addition, the effect of seawater on the pore structure was weakened, and both seawater OPC pastes and DI water OPC pastes exhibited better pore structures.

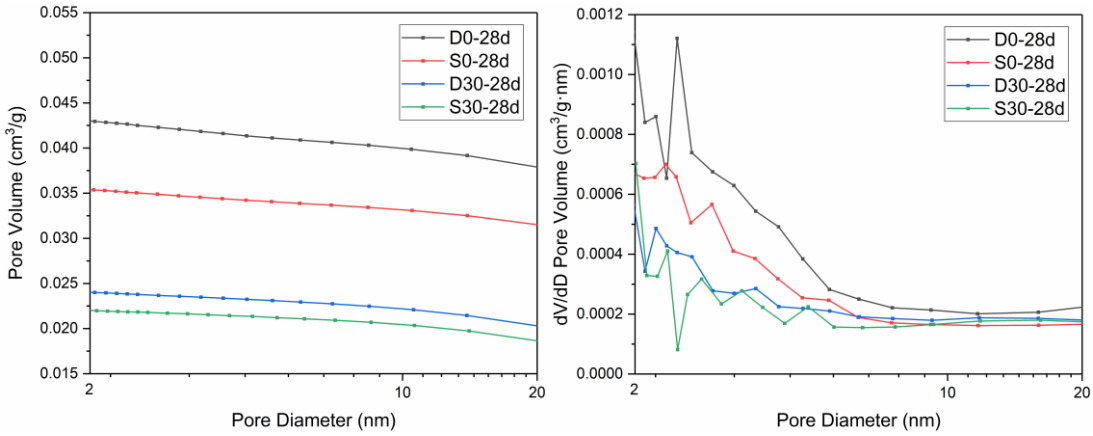

Fig. 11 BJH adsorption curves of different hydrated pastes at 28 days.

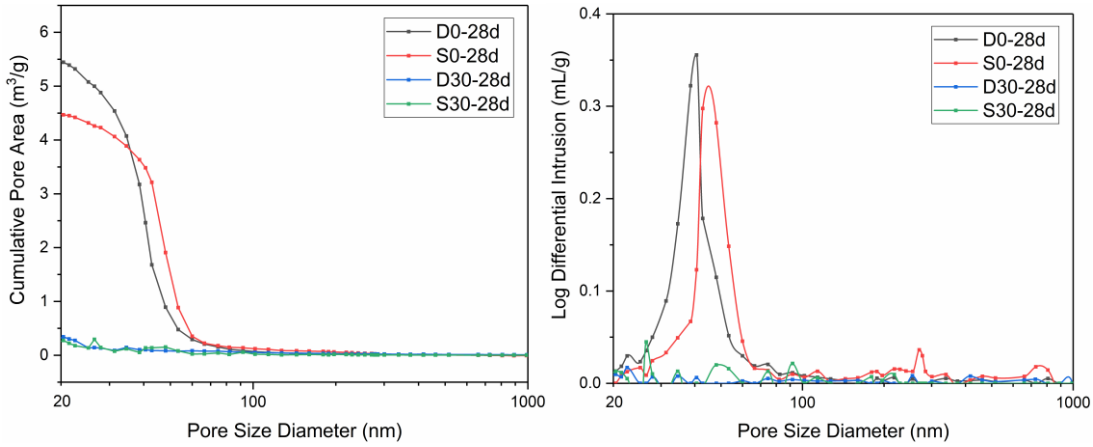

Fig. 12 MIP curves of different hydrated pastes at 28 days.

3.6 Nanoindentation

Nanoindentation analysis was conducted to analyze the micromechanical properties [42-47]. Fig.

13 shows the statistical distribution of indentation modulus in the seawater and DI water OPC-SF systems at 28 days. For OPC pastes with a low W/B, four major phases, namely, LD (low density) C-S-H, HD (high density) C-S-H, UHD (ultra-high density) C-S-H and unhydrated clinkers, can be identified. Generally, the LD C-S-H and HD C-S-H exhibit their intrinsic elastic moduli, which are not dependent on the mix proportions of the specimens [42]. LD C-S-H has been known as an inner product of cement clinker hydration [44], a low stiffness C-S-H [45], or equivalent spheres with random packing (C-S-H globules) [43], with the modulus value ranging from about 17.5 GPa to 27.5 GPa [47]. HD C-S-H has been considered as an outer product [44], a medium stiffness C-S-H [45], or equivalent spheres with more ordered packing [43], with the modulus value ranging from about 27.5 GPa to 33.3 GPa [47]. UHD C-S-H has been reported as a composite of HD C-S-H and nano-CH present in the gel pores of C-S-H [42, 43] with the modulus ranging from about 33.3 GPa to 48.6 GPa [47] and exhibits a relatively high scatter in micromechanical properties due to the CH crystals with various sizes and the possible presence of C_4AF clinkers [43]. Unhydrated cement clinkers exhibits a significantly scattered modulus data (i.e., 48.6 GPa and above [47]) owing to the various sizes of clinker crystals.

The results in Fig. 13 show the seawater OPC pastes and DI water OPC pastes prepared with different SF contents exhibited different distributions of LD C-S-H, HD C-S-H, UHD C-S-H and unhydrated clinkers.

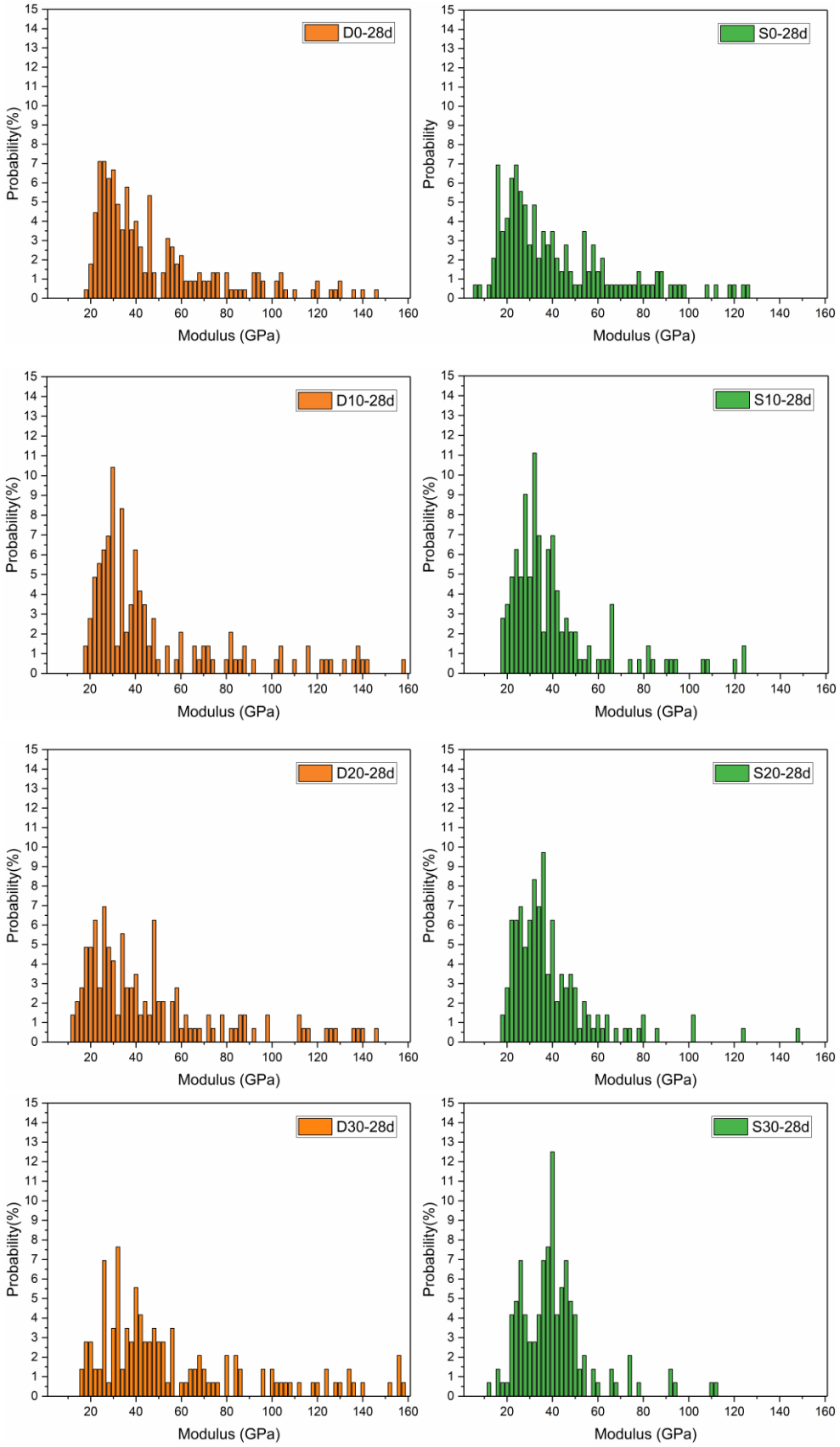

Fig. 13 Statistical distribution of indentation modulus for different hydrated pastes at 28 days.

4. Discussion

The usage of SF changed the influence of seawater on macro-performances and microstructure of OPC pastes prepared with an ultra-low W/B. On the one hand, the compressive strength of seawater OPC-SF system with an ultra-low W/B was increasingly degraded at 28 days as the SF content increased, compared to the DI water OPC-SF system with the same SF addition. The macro-mechanical strength of specimens was closely related to the microstructural evolution. Firstly, the pore structure was not the key factor resulting in the increasing degradation in compressive strength of seawater OPC-SF system. As shown in Figs. 11 and 12, S0 specimen exhibited a poorer pore size distribution compared to the D0 specimen, i.e., larger pore; and thus, the seawater OPC pastes without SF had a lower compressive strength compared to the DI water OPC pastes without SF. However, S30 specimen had a similar pore structure to D30, but the compressive strength of S30 was significantly lower than that of D30. This suggested that the strength reduction in seawater OPC-SF system was not mainly caused by the pore structure.

Fig. 14 shows the volume percentages of unhydrated clinkers and hydration products, based on the difference in indentation modulus, in the hydrated pastes at 28 days. Without SF addition, S0 had a comparable volume percentage of unhydrated clinkers to that of D0; however, the difference in clinker volume between the seawater OPC pastes and DI water OPC pastes became larger as the SF addition increased. Correspondingly, S0 exhibited a slightly low compressive strength compared with D0, but the compressive strength of S30 specimen was significantly degraded compared with D30 specimen, as shown in Fig. 4. Therefore, the change of the amount of

unhydrated clinker phases was the main factor resulting in the macro-strength change, which was because the unhydrated clinkers had a high modulus and exhibited a significantly large scatter in micromechanical properties. Similarly, the Rietveld results and ^{29}Si MAS-NMR results also confirmed the changes in the unhydrated clinkers. As shown in Table 3, the content of unhydrated clinkers in S0 at 28 days was slightly lower than that in D0, however, S30 had a significantly low content of unhydrated clinkers compared with D30. Additionally, as shown in Table 6, S0 sample exhibited a slightly low content of Q^0 distribution compared with D0 sample, but the Q^0 content in S30 was notably lower than that in D30, and correspondingly the content of unhydrated siliceous clinkers showed the same trend.

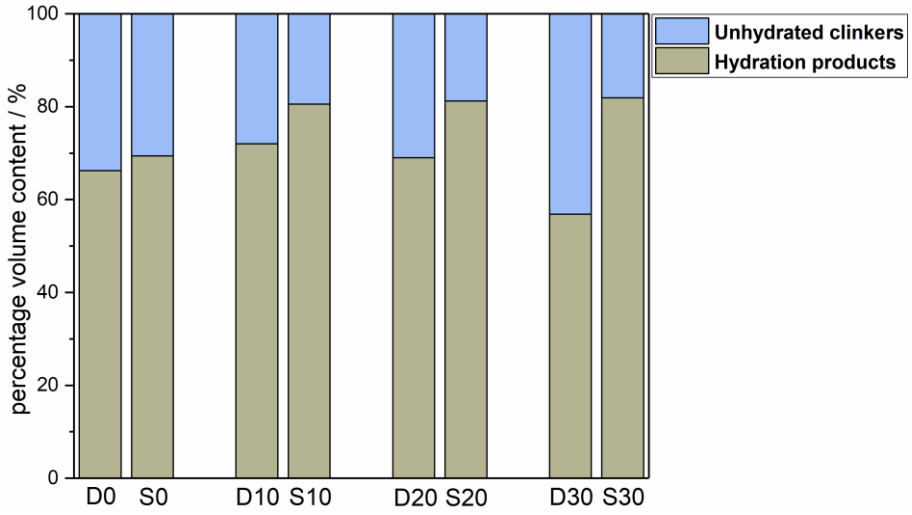

Fig. 14 Volume percentages of clinkers and products at 28 days based on the nanoindentation results

On the other hand, the compressive strength of both the seawater OPC pastes and DI water OPC pastes increased firstly but then decreased with an increase in SF dosage (Fig. 4), which also corresponded to the closest packing results (Fig. 2). The optimal SF dosage was 20% in the DI water OPC pastes. However, for the seawater, the optimal was 10 wt.% SF addition. BSE was used to investigate the pore evolution. Fig. 15 shows the pore size distribution of different

specimens. Image analysis on these hardened pastes was conducted by ImageJ software. The pores were identified by the difference in gray levels from the solid matrix. Pores, unhydrated clinkers and hydrated pastes are shown in different colors in order to clearly distinguish the phases. OPC pastes prepared without SF, regardless of the mixing water used, had more larger pores. The larger pores disappeared and only smaller pores were present when SF was added, suggesting that SF incorporation improved the porosity. The EIS results showed consistent results as the impedance moduli of seawater or DI water OPC-SF systems were notably higher than that of OPC systems prepared without SF, indicating that the OPC-SF system had a denser pore structure and higher external ions corrosion resistance. The average detectable pore contents of DI water OPC pastes were found to be 11.0% (D0), 3.4% (D10), 1.7% (D20) and 4.1% (D30) respectively and D20 had the lowest pore content. D20 also exhibited the highest compressive strength among all the DI water pastes. However, the pore contents of seawater OPC pastes were 9.6% (S0), 2.1% (S10), 3.2% (S20) and 4.5% (S30), respectively, and S10 had the lowest pore content. Thus, the lowest pore content of seawater OPC pastes appeared at a lower SF addition (10 wt%), compared with DI water OPC pastes. A novel concept is proposed to explain this result, i.e., a favorable combination of unhydrated clinkers and different C-S-H gel with varying densities might optimally contribute to the high compressive strength. As shown in Fig. 16, the percentage volume contents of LD C-S-H, HD C-S-H, UHD C-S-H and unhydrated clinkers in S10 sample exhibited a well-proportioned distribution, which is believed to render a high macro-strength. However, the distribution of the different phases in the S30 sample was significantly degraded, i.e., UHD C-S-H accounted for a high percentage and the percentage of HD C-S-H was low.

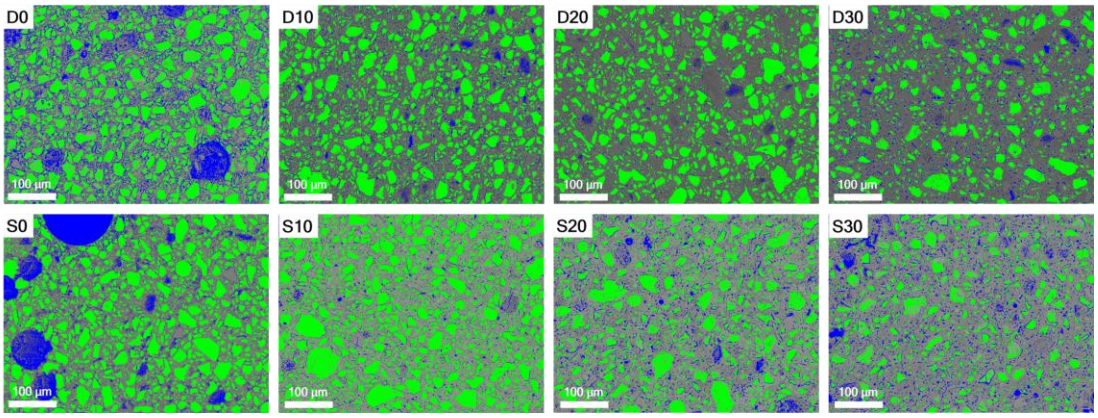

Fig. 15 Pore evolution of DI water OPC pastes and seawater OPC pastes at 28 days based on BSE images. Blue region denoted pore, green region denoted unhydrated clinkers, and grey region denoted hydrated pastes.

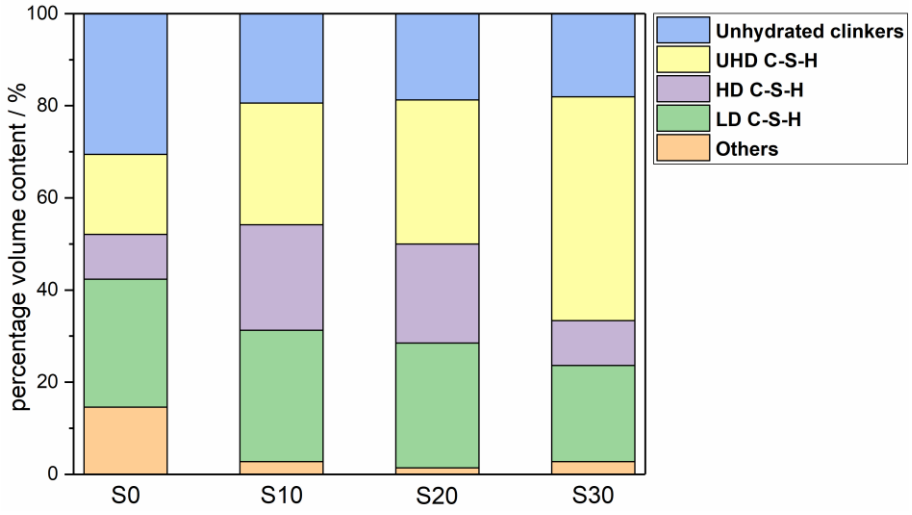

Fig. 16 Volume percentages of different phases in the seawater OPC systems at 28 days

5. Conclusion

The present work investigated the effect of SF on the macro-performances and micro/nanostructure of seawater OPC pastes at an ultra-low W/B ratio. Based on the results of this work, the main conclusions drawn are summarized as follows:

1. With respect to seawater OPC pastes at an ultra-low W/B, the usage of SF was found to enhance

565 the compressive strength at a low SF content. In the seawater OPC-SF system, 10 wt.% SF
566 incorporation exhibited the highest compressive strength while for the DI water OPC-SF system, a
567 20 wt.% SF was needed, and thus the amount of SF dosage might be saved in the seawater based
568 UHPC system.
569
570 2. The durability of the OPC-SF system, regardless of the type of mixing water, was improved
571 with an increase of SF addition. The later-age impedance modulus and external ions corrosion
572 resistance of seawater OPC pastes and DI water OPC pastes increased with the SF content. The
573 seawater OPC pastes exhibited better ions corrosion resistance compared to DI water OPC pastes
574 when 10 wt.% and 20 wt.% SF were used.
575
576 3. The accelerating effect of seawater on cement hydration was small at a later age for the OPC
577 pastes prepared with less than 10 wt% SF addition at an ultra-low W/B. The accelerating effect
578 was still obvious when 30 wt% SF was used. Friedel's salt was not found in the seawater OPC
579 pastes prepared with SF addition. In contrast, the AFt content significantly increased in the
580 seawater OPC-SF system. The polymerization degree and mean molecular chain length of C-S-H
581 gel in both of OPC system and OPC-30%SF system was reduced when seawater was used as the
582 mixing water.
583
584 4. The pore size distribution in the seawater OPC pastes prepared without SF was degraded with
585 more larger pores. However, OPC pastes prepared with SF, regardless of the type of mixing water,
586 exhibited excellent pore structures.

5. The compressive strength of seawater OPC-SF system with an ultra-low W/B was increasingly degraded at a later age with increasing SF addition, compared with the corresponding DI water OPC-SF system, mainly caused by the difference in the distribution of unhydrated clinkers between those two systems. The seawater OPC-10% SF exhibited the highest compressive strength and the lowest pore content among these seawater samples.

Acknowledgments

We wish to thank the financial supports of the Research Grants Council Theme Based Research Scheme (T22-502/18-R), National Natural Science Foundation of China (52108252), Natural Science Foundation of Hebei Province (E2021203147, E2019203413), Key Project of Hebei Education Department (ZD2019096), and Hebei Science &Technology Program (21375401D).

References

[1] J. Xiao, C. Qiang, A. Nanni, K. Zhang, Use of sea-sand and seawater in concrete construction: Current status and future opportunities, Constr. Build. Mater. 155 (2017) 1101-1111.

[2] J.G. Teng, Performance enhancement of structures through the use of fibrereinforced polymer (FRP) composites, Proceedings of 23rd Australasian Conference on the Mechanics of Structures and Materials (ACMSM23), keynote presentation, Lismore, Australia, 2014.

[3] M. Guo, B. Hu, F. Xing, et al., Characterization of the mechanical properties of eco-friendly concrete made with untreated sea sand and seawater based on statistical analysis, Constr. Build. Mater. 234 (2020) 117339.

[4] J. Teng, Y. Xiang, T. Yu, Z. Fang, Development and mechanical behaviour of ultra-high-performance seawater sea-sand concrete, Adv. Struct. Eng. 22 (14) (2019) 3100-3120.

[5] J. Wang, E. Liu, L. Li, Multiscale investigations on hydration mechanisms in seawater OPC paste, Constr. Build. Mater. 191 (2018) 891-903.

[6] H. Zheng, W. Li, F. Ma, Q. Kong, The performance of a surface-applied corrosion inhibitor for the carbon steel in saturated $Ca(OH)_2$ solutions, Cem. Concr. Res. 55 (2014) 102-108.

[7] Y. Zhang, Y. Sun, H. Zheng, Y. Cai, W.L. Lam, C.S. Poon, Mechanism of strength evolution of seawater OPC pastes, Adv. Struct. Eng. 24 (6) (2021) 1256-1266.

[8] P. Li, W. Li, T. Yu, F. Qu, V.W.Y. Tam, Investigation on early-age hydration, mechanical properties and microstructure of seawater sea sand cement mortar, Constr. Build. Mater. 249 (2020) 118776.

[9] S.K. Kaushik, S. Islam, Suitability of sea water for mixing structural concrete exposed to a marine environment, Cem. Concr. Compos. 17 (3) (1995) 177-185.
[10] A. Younis, U. Ebead, P. Suraneni, A. Nanni, Fresh and hardened properties of seawater-mixed concrete, Constr. Build. Mater. 190 (2018) 276-286.
[11] C.G. Girish, D. Tensing, K.L. Priya, Dredged offshore sand as a replacement for fine aggregate in concrete, Int. J. Eng. Sci. Emerg. Technol. 8 (3) (2015) 88-95.
[12] M.M. Islam, M.S. Islam, M. Al-Amin, M.M. Islam, Suitability of sea water on curing and compressive strength of structural concrete, J. Civ. Eng. (the Institution of Engineers, Bangladesh) 40 (1) (2012) 37-45.
[13] T. Nishida, N. Otsuki, H. Ohara, et al. Some considerations for applicability of seawater as mixing water in concrete, J. Mater. Civ. Eng. 27 (7) (2015). B4014004-1-7.
[14] S.A. Yaseen, G.A. Yiseen, C.S. Poon, Z. Li, Influence of seawater on the morphological evolution and the microchemistry of hydration products of tricalcium silicates (C_3S). Acs Sustain. Chem. Eng. 8 (2020) 15875-15887.
[15] P. Sikora, K. Cendrowski, M. Abd Elrahman, S. Chung, E. Mijowska, D. Stephan, The effects of seawater on the hydration, microstructure and strength development of Portland cement pastes incorporating colloidal silica, Appl. Nanosci. 10 (2020) 2627-2638
[16] L. Montanari, P. Suraneni, M. Tsui-Chang, et al., Hydration, pore solution, and porosity of cementitious pastes made with seawater. J. Mater. Civ. Eng. 31(8) (2019) 04019154.
[17] G.C. Edwards, R.L. Angstadt, The effect of some soluble inorganic admixtures on the early hydration of portland cement, J. Appl. Chem. 16 (5) (1966) 166-168.
[18] M. Alkaysi, S. El-Tawil, Z. Liu, et al., Effects of silica powder and cement type on durability of ultra high performance concrete (UHPC), Cem. Concr. Compos. 66 (2016) 47-56.
[19] K. Wille, S. El-Tawil, A.E. Naaman, Properties of strain hardening ultra high performance fiber reinforced concrete (UHP-FRC) under direct tensile loading, Cem. Concr. Compos. 48 (2014) 53-66.
[20] K. Wille, A.E. Naaman, G.J. Parra-Montesinos, Ultra-High Performance Concrete with Compressive Strength Exceeding 150 MPa (22 ksi): A Simpler Way, Aci Mater. J. 108 (1) (2011) 46-54.
[21] C. Shi, Z. Wu, J. Xiao, D. Wang, Z. Huang, Z. Fang, A review on ultra high performance concrete: Part I. Raw materials and mixture design, Constr. Build. Mater. 101 (2015) 741-751.
[22] K. Wille, C. Boisvert-Cotulio, Material efficiency in the design of ultra-high performance concrete, Constr. Build. Mater. 86 (2015) 33-43.
[23] H. Li, N. Farzadnia, C. Shi, The role of seawater in interaction of slag and silica fume with cement in low water-to-binder ratio pastes at the early age of hydration, Constr. Build. Mater. 185 (2018) 508-518.
[24] R. Yu, P. Spiesz, H.J.H. Brouwers, Mix design and properties assessment of Ultra-High Performance Fibre Reinforced Concrete (UHPFRC), Cem. Concr. Res. 56 (2014) 29-39.
[25] J. Zhang, G.W. Scherer, Comparison of methods for arresting hydration of cement, Cem. Concr. Res. 41 (10) (2011) 1024-1036.
[26] B.J. Zhan, D.X. Xuan, C.S. Poon, Enhancement of recycled aggregate properties by accelerated CO_2 curing coupled with limewater soaking process, Cem. Concr. Compos. 89 (2018) 230-237.
[27] W. Ashraf, N. Tian, Nanoindentation assisted investigation on the viscoelastic behavior of carbonated cementitious matrix: Influence of loading function, Constr. Build. Mater. 127 (2016)

904-917.
[28] W. Ashraf, J. Olek, J. Jain, Microscopic features of non-hydraulic calcium silicate cement paste and mortar, Cem. Concr. Res. 100 (2017) 361-372.
[29] M. Santhanam, M. Cohen, J. Olek, Differentiating seawater and groundwater sulfate attack in Portland cement mortars, Cem. Concr. Res. 36 (12) (2006) 2132-2137.
[30] G. Li, A. Zhang, Z. Song, C. Shi, Y. Wang, J. Zhang, Study on the resistance to seawater corrosion of the cementitious systems containing ordinary Portland cement or/and calcium aluminate cement, Constr. Build. Mater. 157 (2017) 852-859.
[31] C. Qiao, P. Suraneni, T. Nathalene Wei Ying, A. Choudhary, J. Weiss, Chloride binding of cement pastes with fly ash exposed to $CaCl_2$ solutions at 5 and 23 °C, Cem. Concr. Compos. 97 (2019) 43-53.
[32] H. Hirao, K. Yamada, H. Takahashi, H. Zibara, Chloride binding of cement estimated by binding isotherms of hydrates, J. Adv. Concr. Technol. 3 (1) (2005) 77-84.
[33] M.V.A. Florea, H.J.H. Brouwers, Chloride binding related to hydration products, Cem. Concr. Res. 42 (2) (2012) 282-290.
[34] K. De Weerdt, A. Colombo, L. Coppola, H. Justnes, M.R. Geiker, Impact of the associated cation on chloride binding of Portland cement paste, Cem. Concr. Res. 68 (2015) 196-202.
[35] U. Ebead, D. Lau, F. Lollini, A. Nanni, P. Suraneni, T. Yu, A review of recent advances in the science and technology of seawater-mixed concrete, Cem. Concr. Res. 152 (2022) 106666.
[36] P. Li, W. Li, Z. Sun, L. Shen, D. Sheng, Development of sustainable concrete incorporating seawater: A critical review on cement hydration, microstructure and mechanical strength, Cem. Concr. Compos. 121 (2021) 104100.
[37] J. Wang, B. Han, Z. Li, et al., Effect investigation of nanofillers on CSH gel structure with Si NMR, J. Mater. Civ. Eng. 31(2018) 04018352.
[38] D. Wang, Y. Fang, Y. Zhang, J. Chang, Changes in mineral composition, growth of calcite crystal, and promotion of physico-chemical properties induced by carbonation of β-C_2S, J. CO_2 Util. 34 (2019) 149-162.
[39] D. Da Silva Andrade, J.H. Da Silva Rêgo, P.C. Morais, A.N. de Mendonça Lopes, M.F. Rojas, Investigation of C-S-H in ternary cement pastes containing nanosilica and highly-reactive supplementary cementitious materials (SCMs): Microstructure and strength, Constr. Build. Mater. 198 (2019) 445-455.
[40] B. Lothenbach, A. Nonat, Calcium silicate hydrates: Solid and liquid phase composition, Cem. Concr. Res. 78 (2015) 57-70.
[41] I.G. Richardson, Model structures for C-(A)-S-H(I), Acta Crystallogr. Sect. B 70 (6) (2014) 903-923.
[42] C. Hu, Z. Li, A review on the mechanical properties of cement-based materials measured by nanoindentation, Constr. Build. Mater. 90 (2015) 80-90.
[43] J. Tatar, C.R. Taylor, H.R. Hamilton, A multiscale micromechanical model of adhesive interphase between cement paste and epoxy supported by nanomechanical evidence, Compos. B Eng. 172 (2019) 679-689.
[44] G. Constantinides, F. Ulm, The nanogranular nature of C-S-H, J. Mech. Phys. Solids. 55 (1) (2007) 64-90.
[45] P. Mondal, S.P. Shah, L. Marks, A reliable technique to determine the local mechanical properties at the nanoscale for cementitious materials, Cem. Concr. Res. 37 (10) (2007) 1440-1444.

[46] L. Li, Z. Li, M. Cao, et al. Nanoindentation and porosity fractal dimension of calcium carbonate whisker reinforced cement paste after elevated temperatures (up to 900°C). Fractals, 29 (2) (2021) 2140001
[47] M. Vandamme, F. Ulm, P. Fonollosa, Nanogranular packing of C-S-H at substochiometric conditions, Cem. Concr. Res. 40 (1) (2010) 14-26